Journal of Sound and Vibration (1999) **224**(3), 431–454
Article No. jsvi.1999.2188, available online at http://www.idealibrary.com on IDEAL®

FORCED VIBRATIONS OF SILOS LEADING TO BUCKLING

FERNANDO G. FLORES AND LUIS A. GODOY

Department of Structures, National University of Córdoba and CONICET, P.O. Box 916, 5000 *Córdoba, Argentina*

(*Received* 25 *August* 1998, *and in final form* 5 *January* 1999)

The large-amplitude force vibrations of steel thin-walled silos when empty are investigated. The basic geometry configuration modelled is a cylinder clamped at the bottom with a top conical roof. Wind pressure distributions are assumed as non-axisymmetric in the circumferential direction and with a rectangular impulse or step distribution in time. Instability is identified from finite-element computations of the time response of the shell using a criterion due to Budianski and Roth. Results are computed for silos made with plain as well as with corrugated sheets, and the influences of geometric imperfections and the stiffening due to the roof are included in the analysis. The problems are also modelled with static pressures using both continuation techniques and bifurcation analysis from a linear fundamental path. Additional results have been obtained to estimate the dynamic buckling load for step loading using energy procedures. All results are computed using finite-element codes developed by the authors.

1. INTRODUCTION

This paper reports on research carried out to elucidate the influence of dynamic effects on the geometric instability of thin-walled metal silos. Wind-load buckling of metal cylindrical silos causes considerable problems in many parts of the world. Failure of such silos is illustrated in the photograph of Figure 1, for a group of empty silos that collapsed in the province of Cordoba (Argentina) in 1993, under wind gusts of 150 km/h. Instability occurs when the silos are empty, and may induce transient deflections in the cylindrical part, in the conical roof, or in both. Wind action is a transient effect which causes forced vibrations of the structure, but the phenomenon of instability may be driven by dynamic effects or may be an essentially quasi-static phenomenon.

The static buckling of cylindrical structures under wind loading has been studied by several authors [1–4]. It is commonly assumed that wind pressure is applied at a slow rate on the structure, so that static bifurcation buckling loads can be computed. A second hypothesis typical of such studies is that the fundamental equilibrium path (the path emerging from the unloaded state) is linear. However, how accurate is a static model for a structural system that is not static?

The evaluation of instability under transient loads requires the computation of the non-linear dynamic response of the structure. A review of forms of evaluation of

0022-460X/99/280431 + 24 $30.00/0

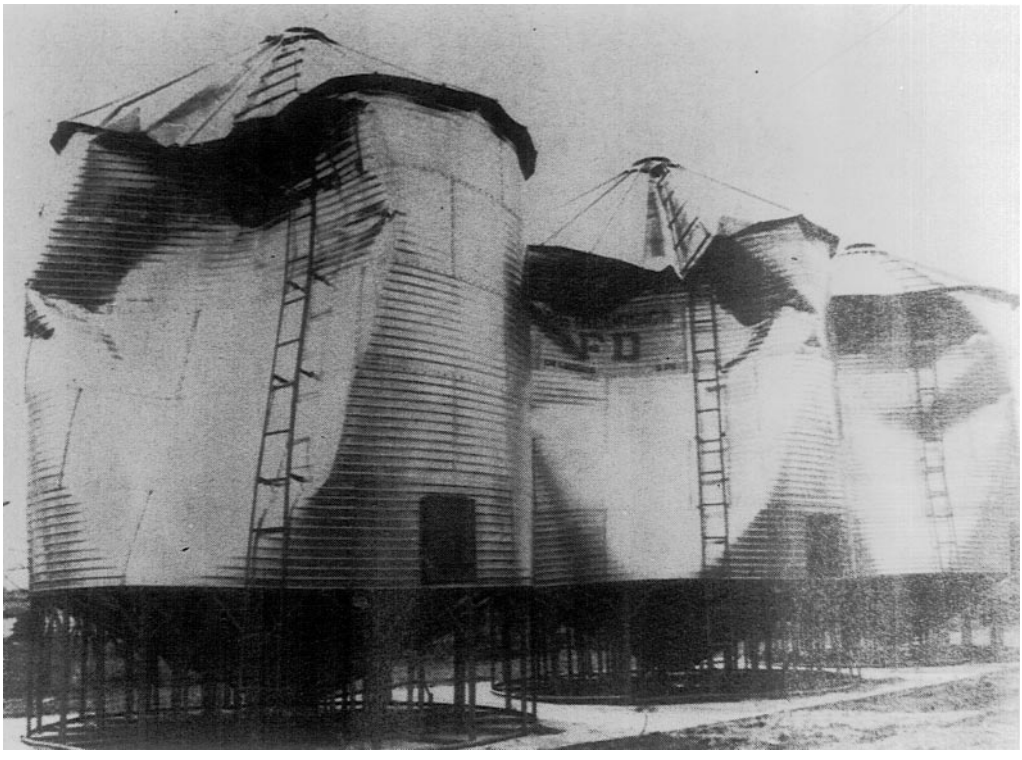

Figure 1. Failure of a group of silos in Colonia Italia, Córdoba (Argentina) in 1993.

instability under suddenly applied loads may be found in the comprehensive work of Simitses [5] and in reference [6]. The most widely accepted criterion of instability under dynamic loads is due to Budianski and Roth [7] and is employed in this paper.

An alternative to estimate buckling under suddenly applied loads is to compute the energy of the system and to infer from it a bound to the dynamic load. Such criterion has been investigated by a number of authors for systems having one or two degrees of freedom, but failed to produce good estimates for multiple degree of freedom systems in typical shell structures employed in tanks [8]. A second objective of this research is to assess the merits of energy approaches to estimate dynamic buckling pressures of such silo systems.

The different formulations employed in the paper are discussed in Section 2, including non-linear dynamic and non-linear static models. The formulations are applied to a theme structure in Section 3, and to the same structure with imperfections and without the roof in Sections 4–6. Sections 7–6 deal with silos with corrugated walls. Conclusions of the studies are presented in Section 10.

2. FORMULATIONS OF THE PROBLEM

In a recent study, the authors considered the forced vibrations and instability of large diameter steel tanks which failed in a Caribbean island [8], and showed that

a step load model could be adequate to represent the time-dependent pressure due to wind. For wind gusts suddenly applied on the structure, the phenomenon of dynamic instability occurred before the end of the wind gusts estimated to have a duration of 3 s. Thus, for shells that reach instability under transient forced vibrations in a very short time, there is no difference between impulsive and step models of pressure, at least for the identification of the onset of dynamic instability. Therefore, the present studies were carried out assuming a space variation of pressure on the shell, and with a step function for the variation in time. Care has been taken in each case to check that the onset of instability occurs within the first few seconds of the transient response.

The wind pressure distribution has been assumed with a circumferential variation in the form

$$p = \Lambda \sum_{i=0}^{7} c_i \cos(\mathrm{i}\theta), \tag{1}$$

where Λ is the scalar parameter employed to increase the pressure, and it is assumed that the meridian of incidence of the wind occurs for $\theta = 0$. Experimental data for the Fourier coefficients in equation (1) for silo structures are not known to the authors; thus in the absence of more detailed experimental evidence, several sets of coefficients were employed from other shell structures. The data employed for the present computations is given in appendix A; however, it was found that the actual pressure distribution in the circumference (and in the height) do no significantly affect the loads at which instability occurs. The same conclusion was found for large diameter tanks as reported in reference [8].

In this work the response has been computed using three computer codes developed by the authors. The first is called ALREF [9] and uses ring elements in a classical shell theory (transverse shear deformations are neglected). It can model non-axisymmetric pressure distributions such as those required for wind loads. This code can predict linear bifurcation loads, non-linear bifurcations loads and asymptotic postcritical paths (non-axisymmetric buckling modes) [10, 11].

The second code is called ALPHA [12]. It is a general-purpose finite-element program. For the silo model, a four-node shell element based upon the theory developed by Simo and coworkers [13–16] was employed. Standard bilinear interpolation is used for the mid-surface and for the director vector (pseudonormal), and an assumed strain formulation is considered for transverse shear deformations. A total Lagrangian formulation has been adopted with objective strain and stress measures (Green–Lagrange strains ε and second Piola–Kirchhoff stresses σ). Corrugated sheets have been modelled using equivalent orthotropic properties [17]. The static module solves the virtual work equation

$$\int_V \delta\varepsilon^{\mathrm{T}} \sigma \, \mathrm{d}V = \int_S \delta\mathbf{u}^{\mathrm{T}} \mathbf{p} \, \mathrm{d}S, \tag{2}$$

where $\delta\mathbf{u}$ are the virtual displacements and $\mathbf{p}$ is the load vector.

In a finite-element formulation, equation (2) becomes "n" algebraic non-linear equations of the form

$$\mathbf{g}(\mathbf{Q}) - \Lambda\mathbf{f} = 0, \tag{3}$$

where the Q_i are the degrees of freedom of the system, $\mathbf{g}$ are the internal nodal equivalent forces and $\mathbf{f}$ are equivalent nodal forces due to the external pressure. The code can follow an elasto-plastic non-linear equilibrium path using standard continuation techniques. It can also predict linear bifurcation loads or can determine the critical point using extended systems [18]. The secondary path can be followed using path switching techniques. For dynamic analysis the inertia terms are added to equation (3) leading to

$$\mathbf{g}(\mathbf{Q}, t) - \mathbf{M}\ddot{\mathbf{Q}} - \Lambda(t)\mathbf{f} = 0. \tag{4}$$

The Newmark algorithm is used to integrate these equations in time, t, where a lumped mass matrix, $\mathbf{M}$ was considered.

The third code is called DELTA [19] and uses the same theoretical basis of the code ALPHA and the same finite elements but it is intended exclusively for transient analysis. The integration in time is performed explicitly in this case using a central difference scheme. This code has been used only in those cases where the implicit code had convergence problems, for example when corrugated silo walls were considered.

The most general criterion of instability available is based on the comparison of the response in time for different load levels [7]. The procedure consists in finding the load parameter Λ_D so that for small changes in the load Λ, there are large changes in the response (displacements) of the system. This is a very general procedure, and does not involve approximations other than the numerical accuracy in the computation of the response in time. The procedure calls for the evaluation of the non-linear dynamic response at a number of load levels.

A second study presented in the following sections is based on the response in the phase space. In the phase space the transient displacements are plotted versus velocities. If attention is restricted to just one degree of freedom of the system and its corresponding velocity, then the evolution in time leads to cycles in this space. Instability occurs if for one of the generalized co-ordinates of the system both the velocity and the acceleration become zero.

A third study is presented to estimate dynamic instability under step loading (as in the present modelling of pressures) using the static non-linear equilibrium path and the total potential energy V. The procedure was originally developed by Hoff and Bruce [20] and extended by several researchers [21–23, 6]. In the present case, the non-linear equilibrium path has been computed using continuation techniques with increments in displacements, under the same pressure defined in Appendix A but applied as a static action. The equilibrium path satisfies the condition

$$\frac{\partial V}{\partial Q_i} = 0. \tag{5}$$

On the unstable part of the path, instability under step load occurs whenever the energy, V, becomes zero:

$$V = 0. \tag{6}$$

In this paper, the energy has been computed along with the continuation analysis, until the condition (6) is satisfied.

A fourth study carried out is a static bifurcation analysis of the shell under wind load action. The fundamental equilibrium path (emerging from the unloaded state) is assumed to be linear, and a bifurcation load is computed using ALREF.

The complete set of four studies gives a more comprehensive understanding of the instability phenomenon of silos under simulations of wind action than what would be obtained from any individual study. Also the comparison between dynamic and static analysis allows to understand the importance of inertia effects in this problem.

3. CASE STUDY

We start the analysis of results for a silo structure with dimensions shown in Figure 2. This is a cylindrical silo, almost 16 m in diameter, with variable thickness. This silo geometry was previously studied by Ruiz [24] regarding a structural collapse. Typical deflections at the onset of buckling are shown in Figure 3, in the circumferential direction and in elevation. As the cylinder buckles (computed from the static analysis) only the cylindrical part has deflections and the conical part remains unaffected, thus providing stiffening to the structure. Deflections are not significant in the lower part of the cylinder, where the thickness is largest. The deflections in the circumferential direction are localized within 30° from the meridian of incidence of the maximum wind pressure.

The transient response of the shell at the location of maximum deflection is shown in Figure 4(a). For a load parameter $\Lambda = 1360{\cdot}3$ the vibrations of the shell are stable. However, a small variation in the amplitude of the step load from 1360·3 to 1367·2 produces a large change in the response, so that the displacements have large changes which are not proportional to the small change in the load. Dynamic buckling under the current simulation of wind load is thus obtained by refining the change in the load, and is found to occur at $\Lambda_D = 1367$. The time required to have instability is less than 1 s, so that a step model in time leads to the same value of dynamic buckling load is a rectangular impulse with the same pressure distribution and duration of 3 s.

The evolution of the system can also be followed in the phase space, as indicated in Figure 4(b). Here the system has a number of cycles before instability occurs. The critical load is reached when the velocity and the acceleration of a one-degree-of-freedom system are both zero. This criterion was extended to multiple-degree-of-freedom systems by Raftoyiannis and Kounadis [25], so that instability is identified in one generalized co-ordinate when both the velocity and the acceleration are zero. Such criterion has not been employed in this work

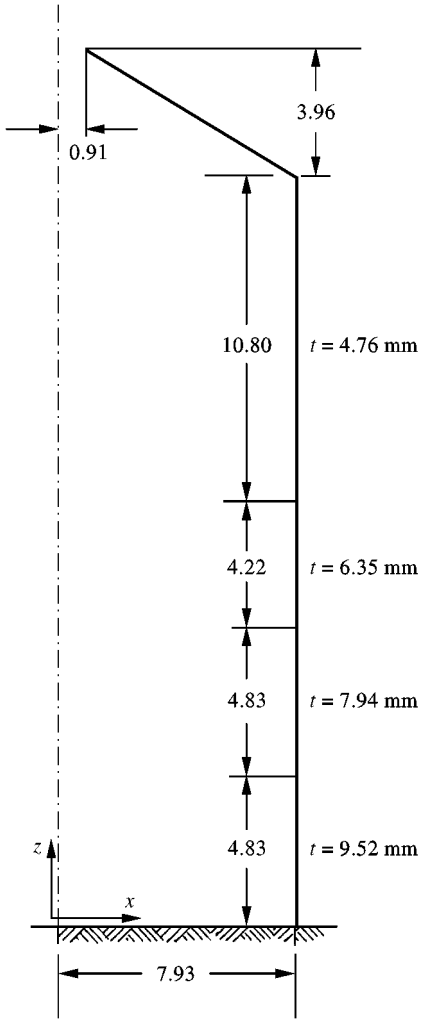

Figure 2. Silo made of a plain wall and different thicknesses.

because of its computational cost: to identify the zero values of velocity and acceleration one has to refine the load at which instability occurs, mainly because the acceleration is very sensitive to small changes in the load. Identification of instability in the time domain, on the other hand, is a rather simple matter, even if the load is in the vicinity of the exact value for dynamic instability.

Having considered the forced vibrations of the shell, attention is now given to the static non-linear response of the structure. Consider the point of maximum deflection in Figure 3; then, the static load-deflection equilibrium path is shown in Figure 5. The initial part of the path is clearly linear, and the maximum load attained is reached at $\Lambda_C = 1381$, with displacements of 20 mm. The postcritical part of the path is descending, and a recovery of stiffness is found for large deflections. A linear bifurcation model has also been employed, leading to a bifurcation load $\Lambda_C^{\text{linear}} = 1285$, with maximum displacements of 10 mm.

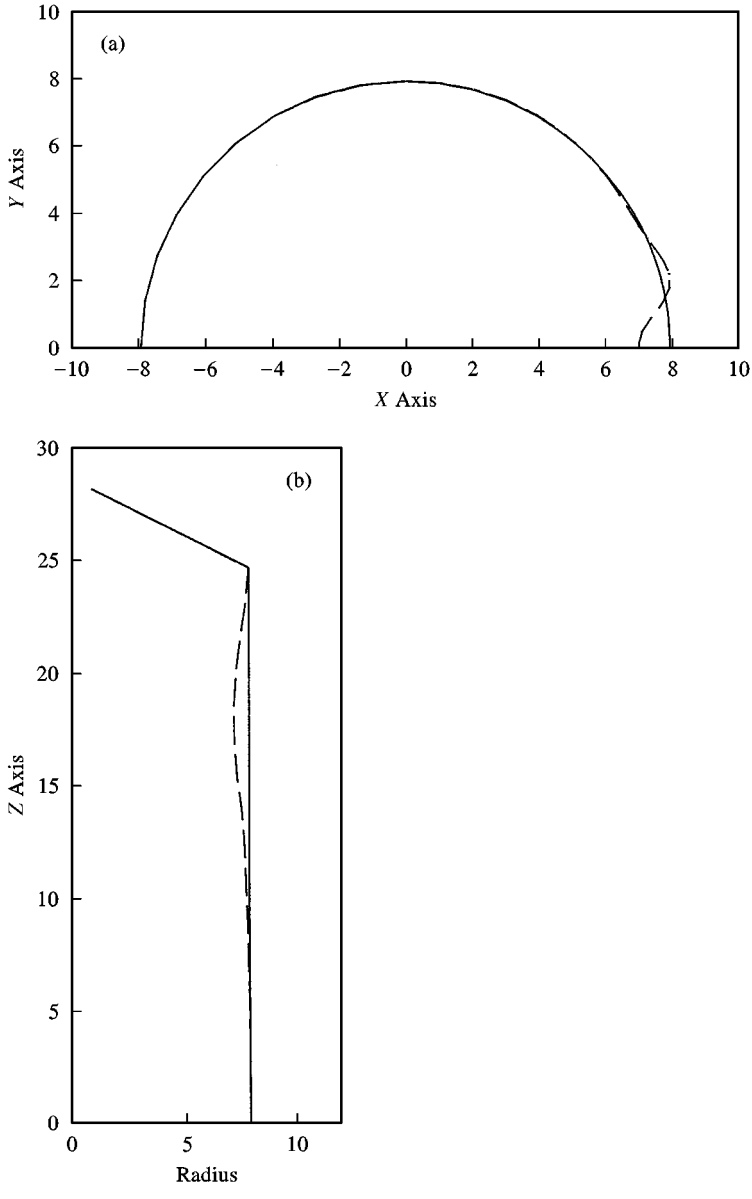

Figure 3. Buckling mode of the plain-wall silo: (a) circumferential mode at $z = 17{\cdot}48$ m, (b) buckling profile at $\theta = 0$; —, original geometry; ---, deformed geometry.

The components of the energy evaluated along the non-linear equilibrium path may provide important information about the behavior of the system. The energy contributions of the static system are also plotted in Figure 5 as a function of displacements. Notice that the total potential energy of the system is never zero although it comes close to this value for a displacement of 120 mm. The consequence is that the energy criterion cannot be employed in this case to estimate the dynamic buckling load under step loading.

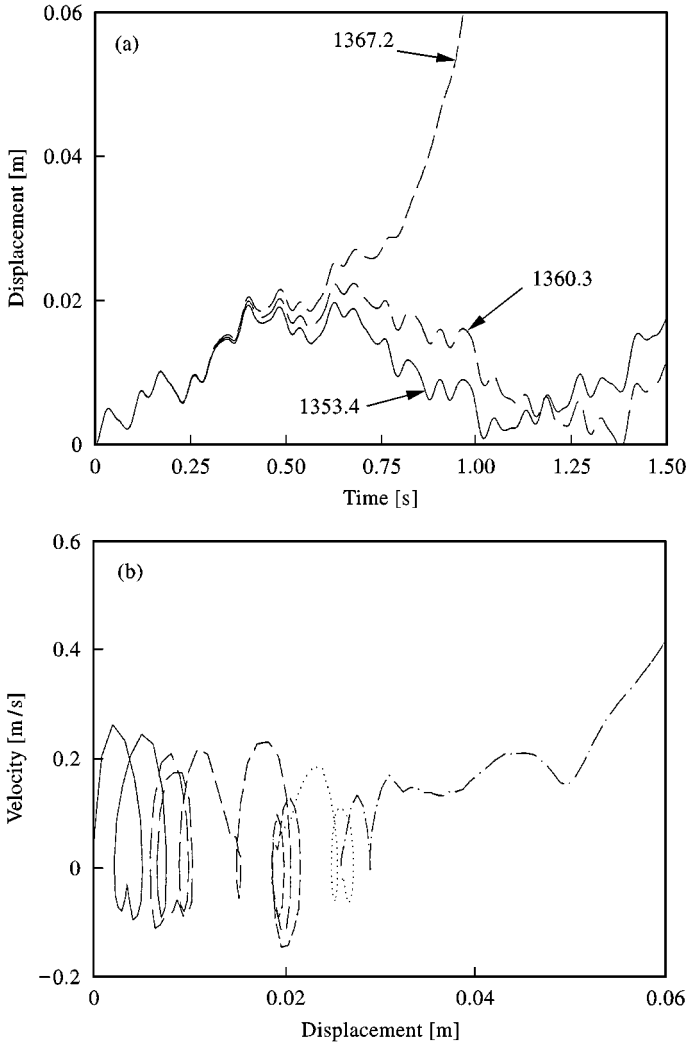

Figure 4. Transient analysis of the plain-wall silo: (a) displacement at the location of maximum amplitude for different step load levels; (b) movement in the phase space for $\Lambda = 1367{\cdot}2$

In the present study, the transient response of the shell leads to instability for a load which is 98% of the value in the non-linear static analysis. Thus, it seems that inertia effects are not very significant in affecting the response of the shell. The static prediction in this case is a good estimate of dynamic instability.

A second observation is that bifurcation buckling is a reasonable approximation of the non-linear geometric behavior for the present case, with an error in the static critical load of 7%.

4. INFLUENCE OF GEOMETRIC IMPERFECTIONS

The instability of thin-walled structures is known to be sensitive to small imperfections in the geometry. In the present case, the same silo of Figure 2 has

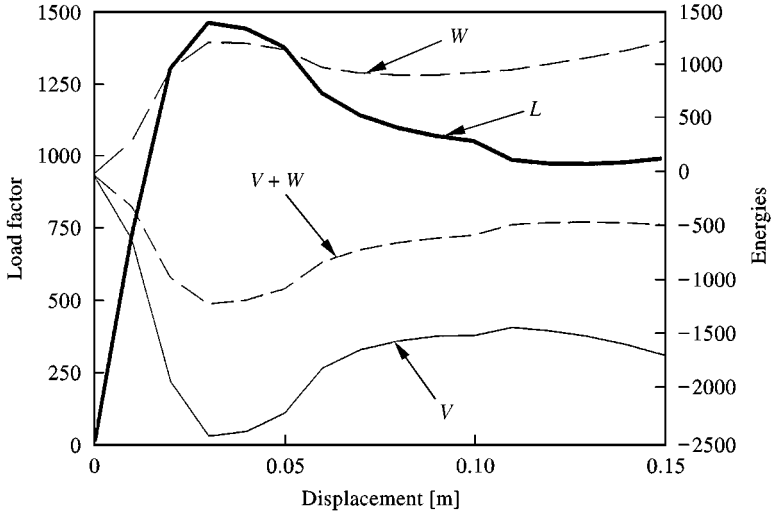

Figure 5. Static analysis of the plain-wall silo. (L) Load–displacement equilibrium path; (V) potential of the external loads; (W) internal strain energy.

been investigated with a number of geometric deviations, and one such study is reported here. The specific shape deviation has the same geometry as the static buckling mode calculated from the bifurcation analysis, and with maximum amplitude of 5 mm (slightly larger than the minimum thickness).

Computation of the transient response is shown in Figure 6(a) for the imperfect shell, and the results should be compared with those of Figure 4(a) for the perfect shell. In the imperfect shell, dynamic buckling occurs for a load parameter of $\Lambda = 985$, that is a decrease of 28% with respect to values in the perfect shell ($\Lambda = 1367$). The time at which instability starts is also less in the imperfect shell by almost 50% (a more accurate value of the time at buckling requires a refinement of the load step employed to increase the load between different transient computations; however, the exact value is smaller than the approximate one). Next, static values were computed for the imperfect shell, leading to a maximum load $\Lambda = 1060$. This means that instability detected using the dynamic criterion yields values of 93% of the static limit load.

It seems clear that imperfections affect the response of the shell regarding the computation of dynamic buckling loads, and should thus be taken into account. For an imperfection with a maximum amplitude of the order of the thickness, the reduction in dynamic buckling load was of 28%. As in the perfect case, the dynamic buckling process can be approximated by means of an imperfect static non-linear analysis, with errors in maximum load of about 7%.

5. INFLUENCE OF THE GEOMETRY OF THE SILO

The silo of Figure 2 is representative of a range of silo constructions, but shorter silos with larger diameters are also employed as an alternative. Consider

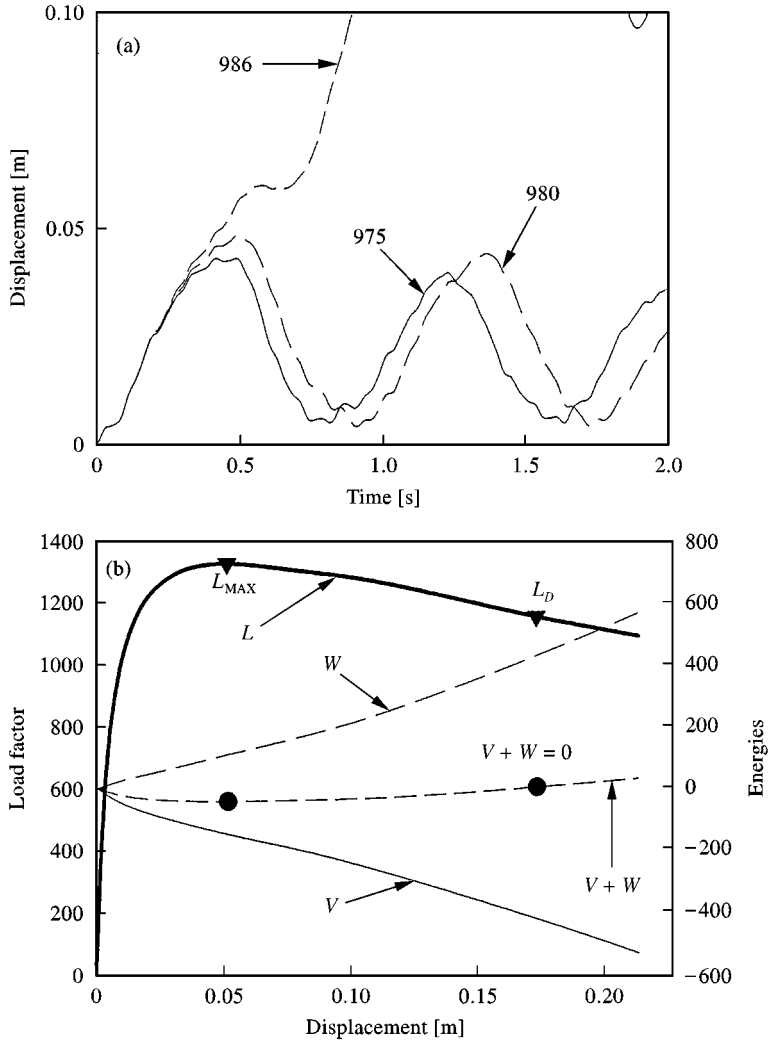

Figure 6. Analysis of the imperfect silo with plain wall: (a) transient analysis at the leading edge for different load levels; (b) static analysis.

a geometry with $R = 12{\cdot}1$ m, $H = 8{\cdot}64$ m and $t = 6{\cdot}35$ mm, with a constant thickness in elevation.

The transient response of the shell is shown in Figure 7 and indicates that buckling under an impulsive load occurs before the first 3 s of response. The actual value of the load at instability is estimated as $\Lambda = 1537$, a higher value than in the first silo of Figure 2. The number of cycles before buckling in this case is increased, as shown in Figure 7(a). The static response of the shell is shown in Figure 7(b), and for this case the maximum load is $\Lambda = 1585$, which is reached with small displacements (about 15 mm).

For this large diameter shell, the static criterion based on energy considerations is applicable. The energy becomes zero in correspondence with a load $\Lambda = 1275$.

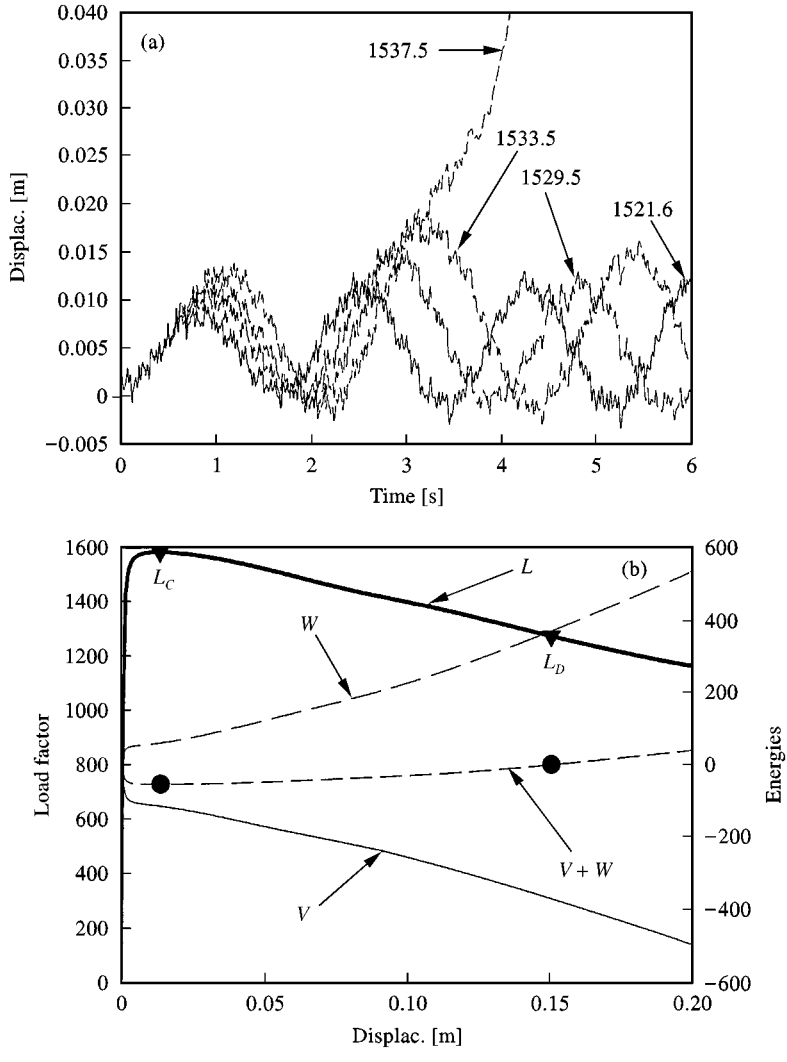

Figure 7. Short silo without the roof. (a) transient analysis at the leading edge for different load levels; (b) static analysis. (L) load–displacement equilibrium path; (V) potential of the external loads; (W) internal strain energy.

This latter value is the static estimate using the energy criterion, and is seen to represent a conservative value with respect to the dynamic load at buckling.

The same shell has been studied including the influence of imperfections, and results for imperfection amplitude of 5 mm are shown in Figure 8(a), (b). The transient response indicates instability at $\Lambda = 1237$, at a time of about 0·6 s. Comparison with results of the perfect shell show a decrease of 20% due to imperfections, and a significant reduction in the time required for buckling.

The static response of the imperfect shell yields $\Lambda = 1327$, which is in close agreement with the results from the dynamic analysis.

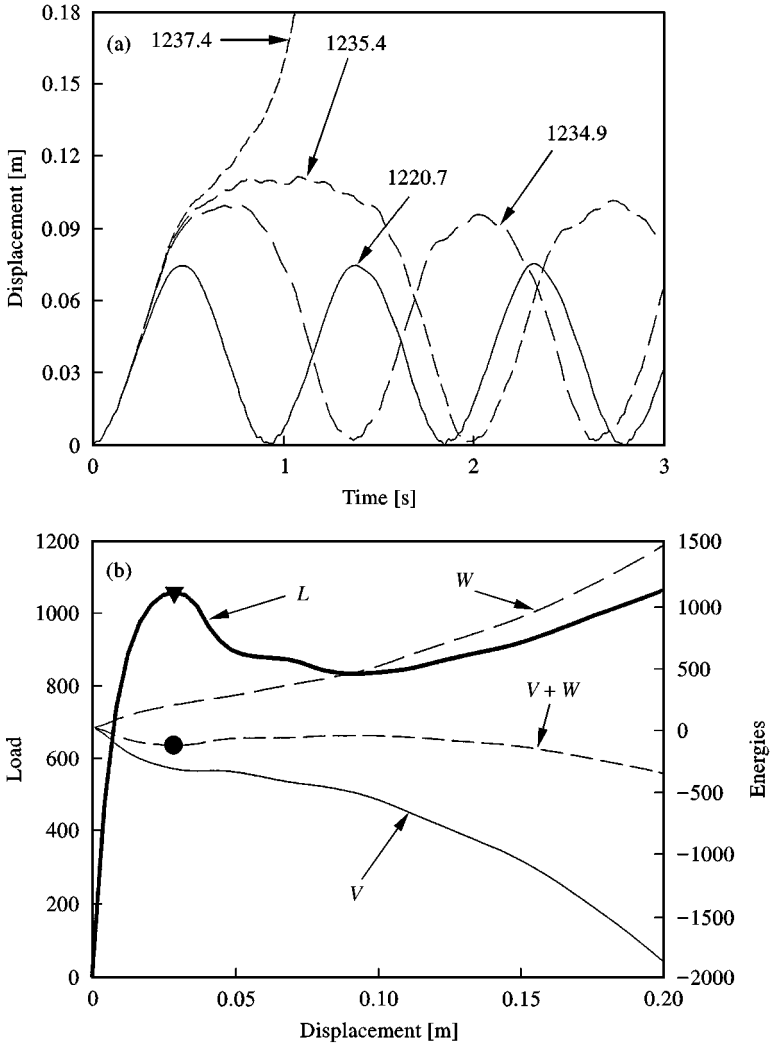

Figure 8. Imperfect short silo without the roof: (a) transient analysis at the leading edge for different load levels: (b) static analysis. (L) Load–displacement equilibrium path; (V) potential of the external loads; (W) internal strain energy.

Again, it is possible to employ the energy criterion for step load buckling, but the results are too conservative.

6. SILO WITHOUT THE ROOF

The behavior of a silo without the roof is illustrated in this section for the same silo geometry of Section 3. Loss of the conical part of the silo during the early stages of wind action may occur due to inadequate joints between the cylindrical part and the cone, and the consequences of the forced vibrations of the remaining silo are investigated here.

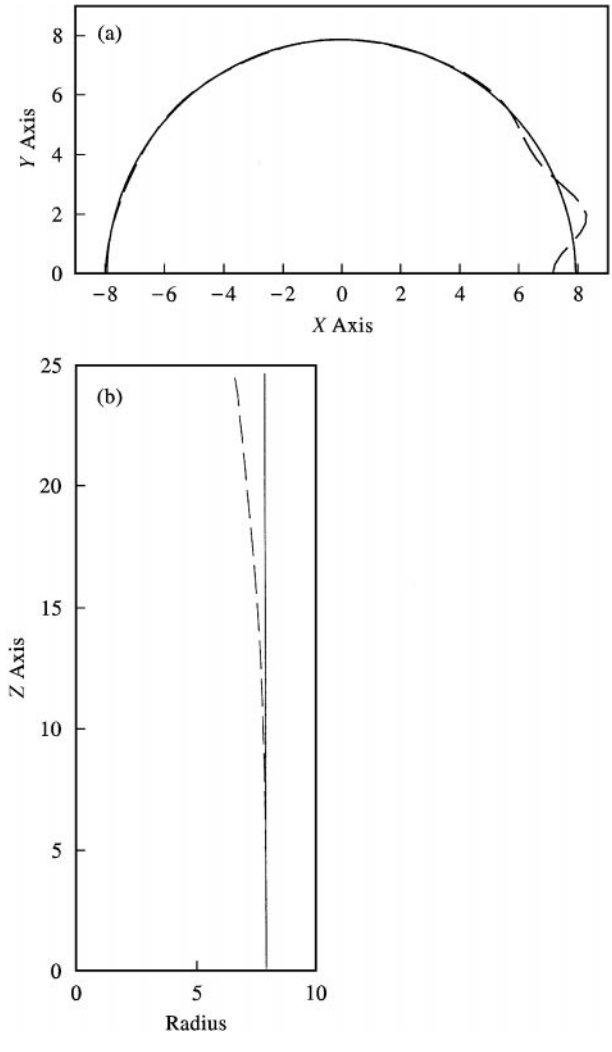

Figure 9. Static buckling mode of the plain-wall silo without the roof: (a) circumferential mode at the free edge (b) buckling profile at $\theta = 0$; —, original geometry; ----, deformed geometry.

The static deformations are shown in Figure 9. The zone affected at the onset of static buckling is larger than in the complete silo, and the difference between non-linear static instability ($\Lambda_C = 600{\cdot}8$) and bifurcation from a linear fundamental path ($\Lambda_C^{\text{linear}} = 731{\cdot}2$) is larger than in Section 3.

The forced vibrations of the system are shown in Figure 10(a). Unstable behavior starts at approximately 1·5 s, and occurs at a load $\Lambda = 584$ and displacements of the order of 40 mm. This load is much lower than the dynamic buckling load for the complete silo. The stiffening influence of the roof is lost in this case, so that the shell becomes unstable at about 50% of the dynamic buckling load of the complete silo. It is thus very important to design the joint in such a way that the integrity of the silo is preserved at all times and that the joint fails for loads higher than instability of the silo.

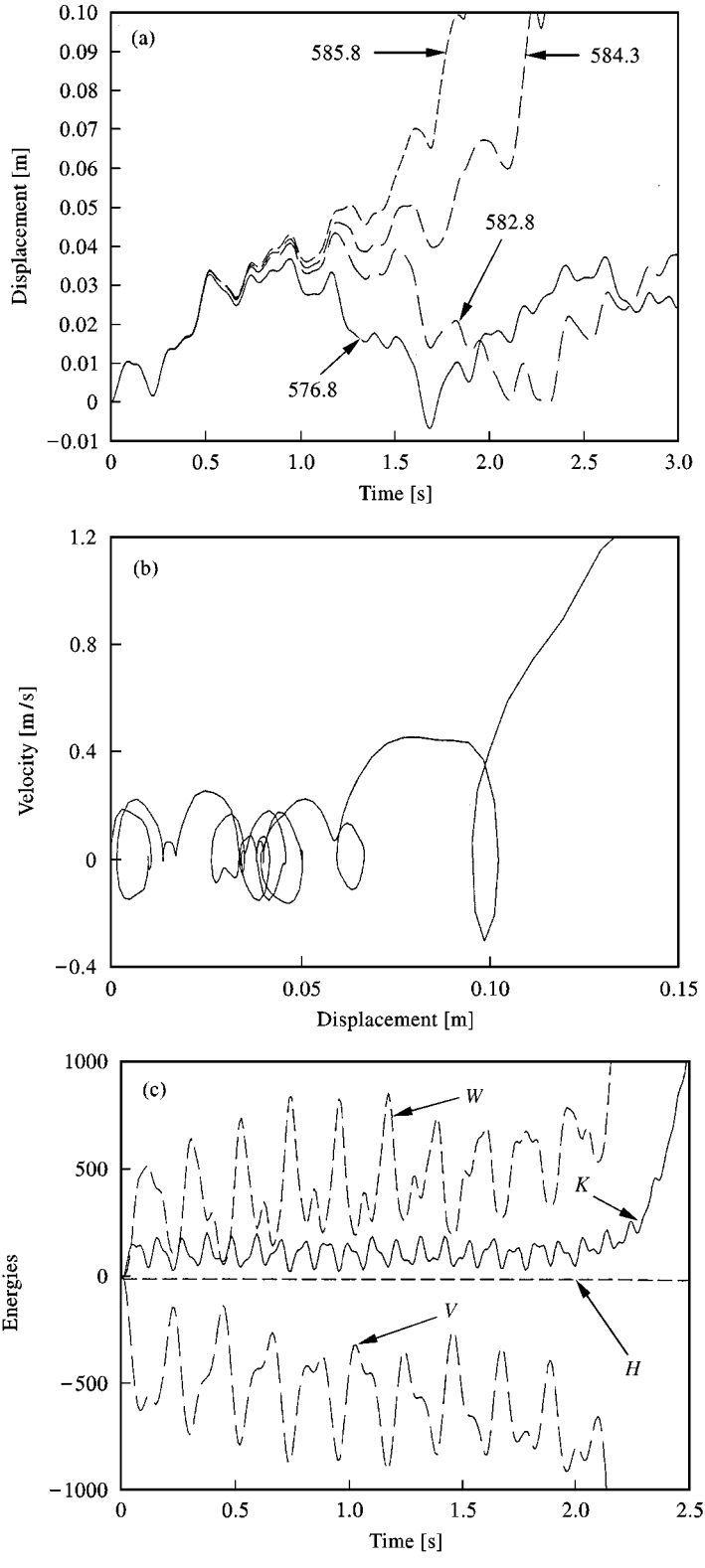
(a)
585.8
584.3
582.8
576.8
Displacement [m]
Time [s]
(b)
Velocity [m/s]
Displacement [m]
(c)
W
K
V
H
Energies
Time [s]

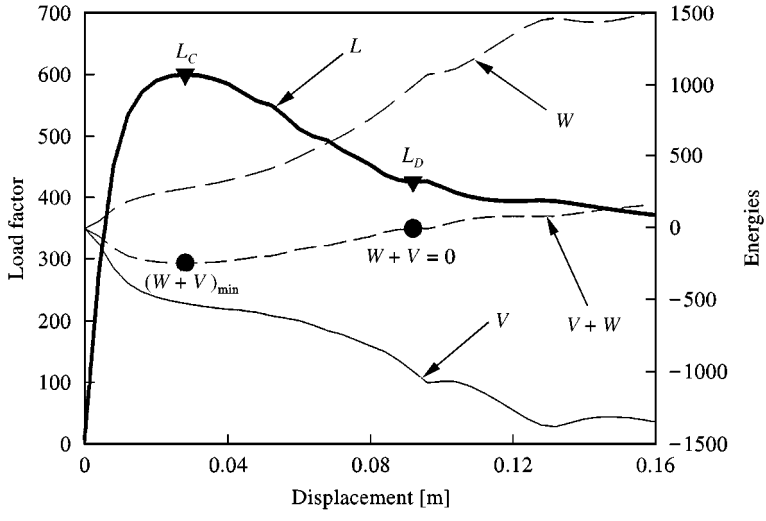

Figure 11. Static analysis of the plain wall silo without the roof. (L) Load–displacement equilibrium path; (V) potential of the external loads; (W) internal strain energy.

The cycles in the phase space are shown in Figure 10(b). Again, for this multiple-degree-of-freedom system it is not possible to observe the condition of both velocity and acceleration equal to zero at the onset of instability unless the load step is refined.

The energy components are not constant during the transient response, except for the Hamiltonian, which is zero at all times. The non-linear oscillations of the system produce exchanges of energy from potential to kinetic energy. The levels of kinetic energy K in Figure 10(c) are smaller than those due to elastic deformations and the load potential.

The static non-linear response of the shell has been computed and results are shown in Figure 11. The system has important non-linear effects prior to reaching a critical state at $\Lambda_C = 600{\cdot}8$ and displacements of 30mm.

The energy contributions of the static system are also shown in Figure 11, and they are such that for a displacement of about 80 mm, the total potential energy becomes zero. Thus, it is possible in this case to apply the approximate energy criterion for a step load. In the present case the load on the descending part of the non-linear equilibrium path for which $V = 0$ is $\Lambda_D = 424$, a much lower value than the instability load using the transient response. The energy criterion of step loading is too conservative in this case.

7. SILO WITH CORRUGATED WALLS

A very common silo construction is made using corrugated curved plates, so that it is important to evaluate how such wall shape influences the forced vibrations of

Figure 10. Transient analysis of the silo without the roof: (a) displacement of the top point a the leading edge for different load levels; (b) movement in the phase space for $\Lambda = 584{\cdot}2$; (c) evolution of energy components for $\Lambda = 584{\cdot}2$, international strain energy, W; kinetic energy, K; potential of external loads, V; Hamiltonian H.

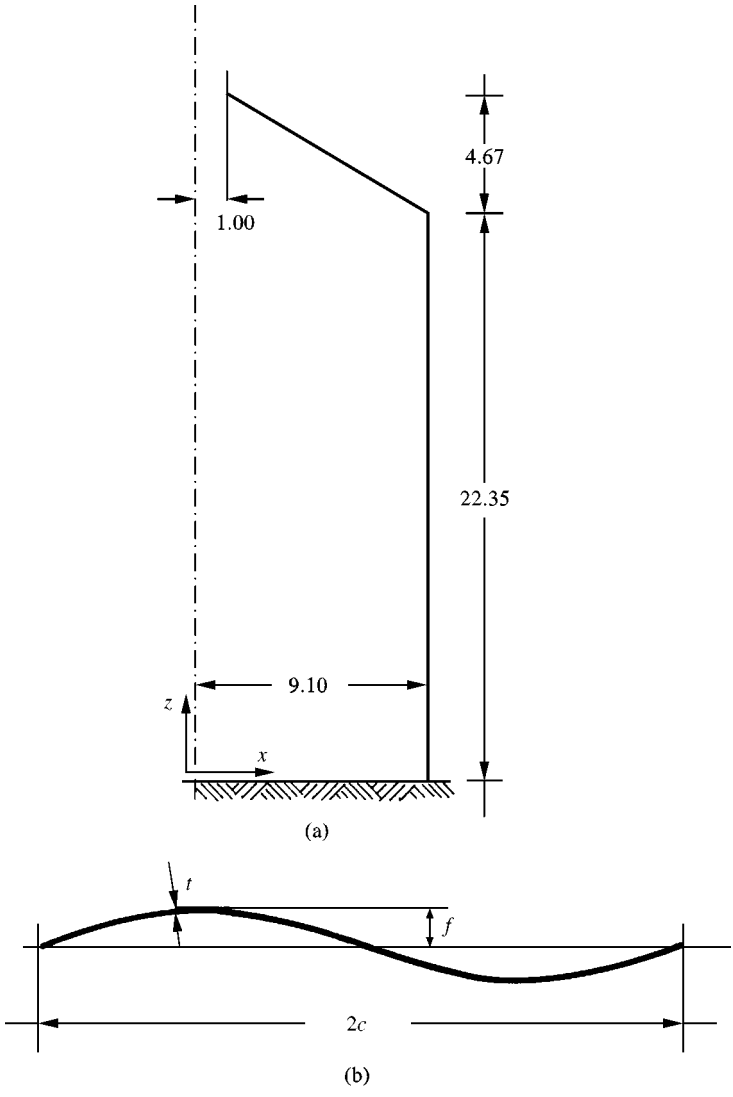

Figure 12. Silo made of corrugated panels: (a) global geometry and (b) details of the wall ($zc = 10{\cdot}16$ cm, $f = 0{\cdot}556$ cm, $t = 0{\cdot}35$ cm)

the silo. The geometry and wall properties have been taken from a European firm operating in Argentina, and are shown in Figure 12. The waves on the walls are very short compared with the buckling mode, shown in Figure 13. Again, the complete silo has deflections restricted to the cylindrical part at static buckling. In this case, the thickness is constant and the deflections in elevation affect a much larger zone than in Figure 3(a). The transverse deflections affect a wider zone in the circumferential direction and this is a consequence of the higher stiffness of the wall.

The transient response of the silo is shown in Figure 14(a). Stable behavior is found for $\Lambda = 1625$; however, unstable response is observed for $\Lambda = 1641$. The

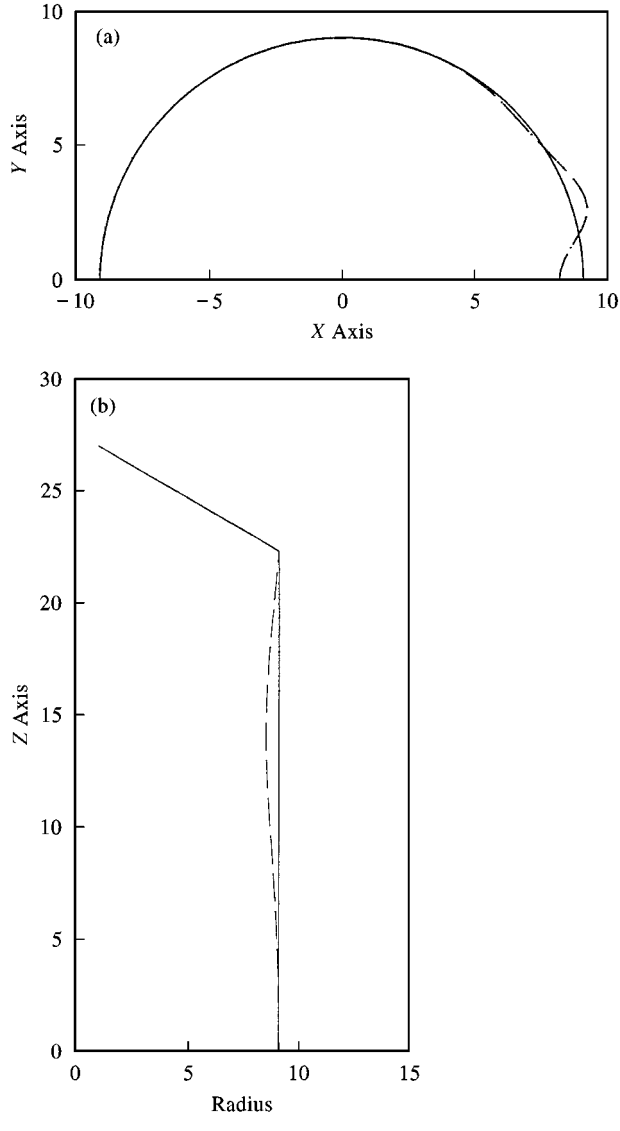

Figure 13. Static buckling modes: (a) circumferential mode at $z = 15{\cdot}5$ m, (b) buckling profile at $\theta = 0$; —, original geometry; ---, deformed geometry.

phase-space evolution of the system is shown in Figure 14(b) for the point of maximum static deflection.

The non-linear static response is plotted in Figure 15. The influence of non-linearity on the fundamental equilibrium path is important in this case, and leads to a critical load $\Lambda = 1675$ with displacement amplitude of 90 mm. The static bifurcation load is much higher, reaching $\Lambda_C^{\text{linear}} = 3487$. The static energy components are also plotted in Figure 15, and do not become zero for any displacement configuration. Thus, the approximate energy criterion cannot be applied in this silo configuration.

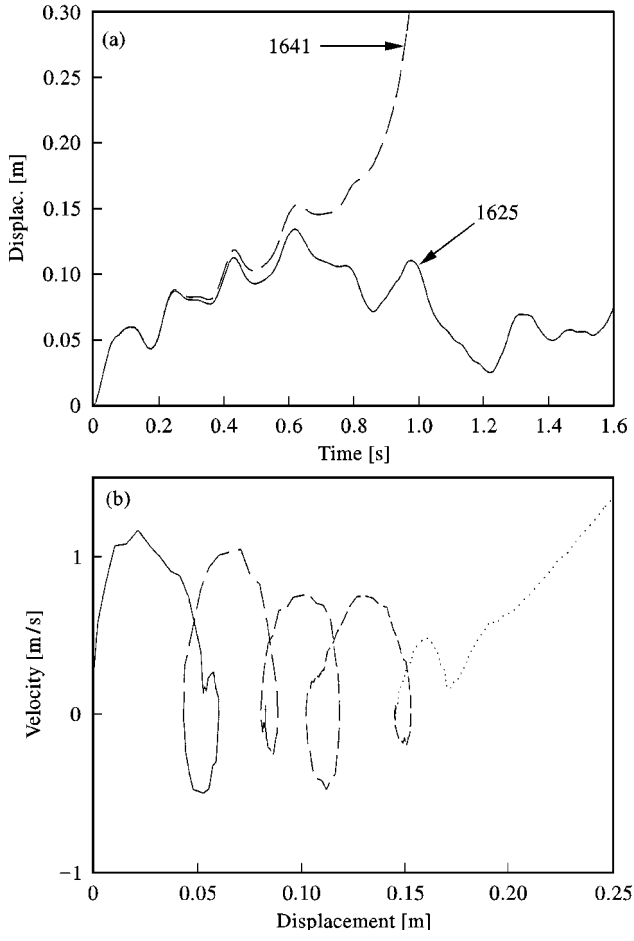

Figure 14. Transient analysis of the silo with a corrugated wall: (a) displacement of point at $z = 15{\cdot}5$ cm on the leading edge, (b) movement of the point in phase space.

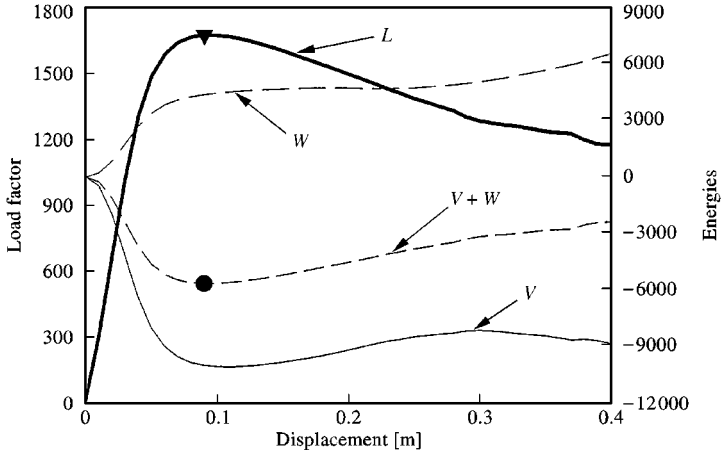

Figure 15. Static analysis of the silo with a corrugated wall. (L) Load–displacement equilibrium path; (V) potential of the external loads; (W) internal strain energy.

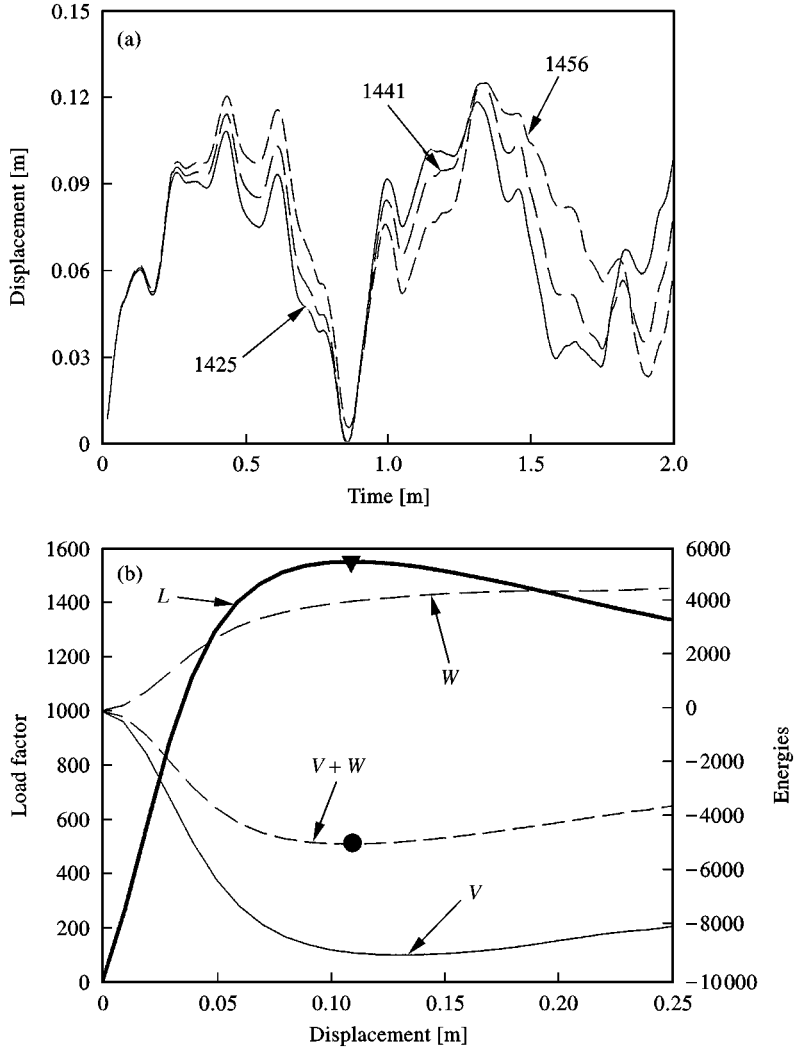

Figure 16. Imperfect silo with a corrugated wall: (a) transient analysis at the leading edge for different load levels; (b) static analysis. (L) Load–displacement equilibrium path; (V) potential of the external loads; (W) internal strain energy.

8. INFLUENCE OF GEOMETRIC IMPERFECTIONS IN CORRUGATED SILOS

How imperfections affect the dynamic response of corrugated wall silos has been investigated for one case. The transient response of the shell with amplitude of imperfection of 5 mm is shown in Figure 16(a). Instability in this case is detected for $\Lambda = 1456$, a reduction of 11% with respect to the value obtained for the perfect shell.

The non-linear static response is plotted in Figure 16(b) and displays a maximum in the load at $\Lambda = 1549$. The dynamic buckling load in this case is 94% of the static value.

9. INFLUENCE OF THE ROOF IN CORRUGATED SILOS

A silo with similar wall characteristics as in Figure 12 with $R = 9{\cdot}1$ m, $H = 5{\cdot}59$ m and without the roof has been investigated. The dynamic criterion of stability of Budianski–Roth has been used in Figure 17(a) to evaluate instability and results in dynamic buckling at $\Lambda = 2990$, and for a time exceeding 3 s.

Small differences in the vibrations of the shell are obtained in this case between an impulsive load with 3 s duration and a step load, but the dynamic buckling load is the same.

Computation of the equilibrium path using the static model is shown in Figure 17(b), with a maximum load at $\Lambda = 3115$ and displacements of the order of 70 mm.

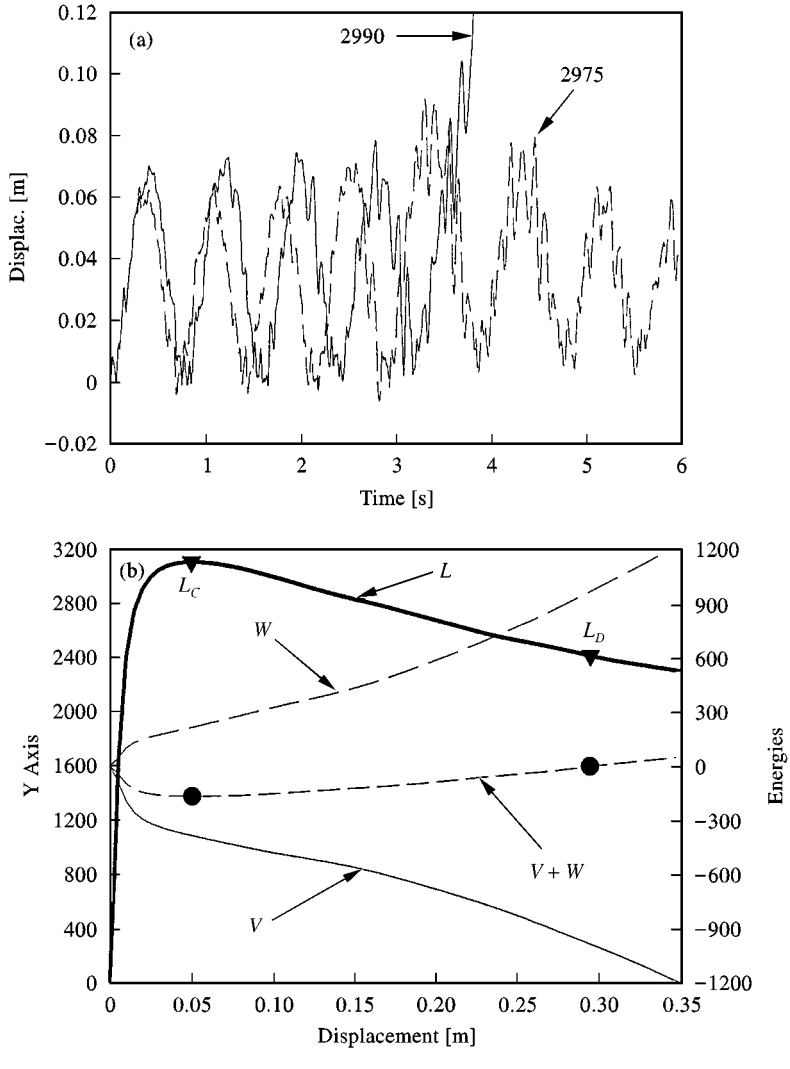

Figure 17. Short corrugated wall silo without the roof: (a) transient analysis at the leading edge for different load levels; (b) static analysis. (L) Load–displacement equilibrium path; (V) potential of the external loads; (W) internal strain energy.

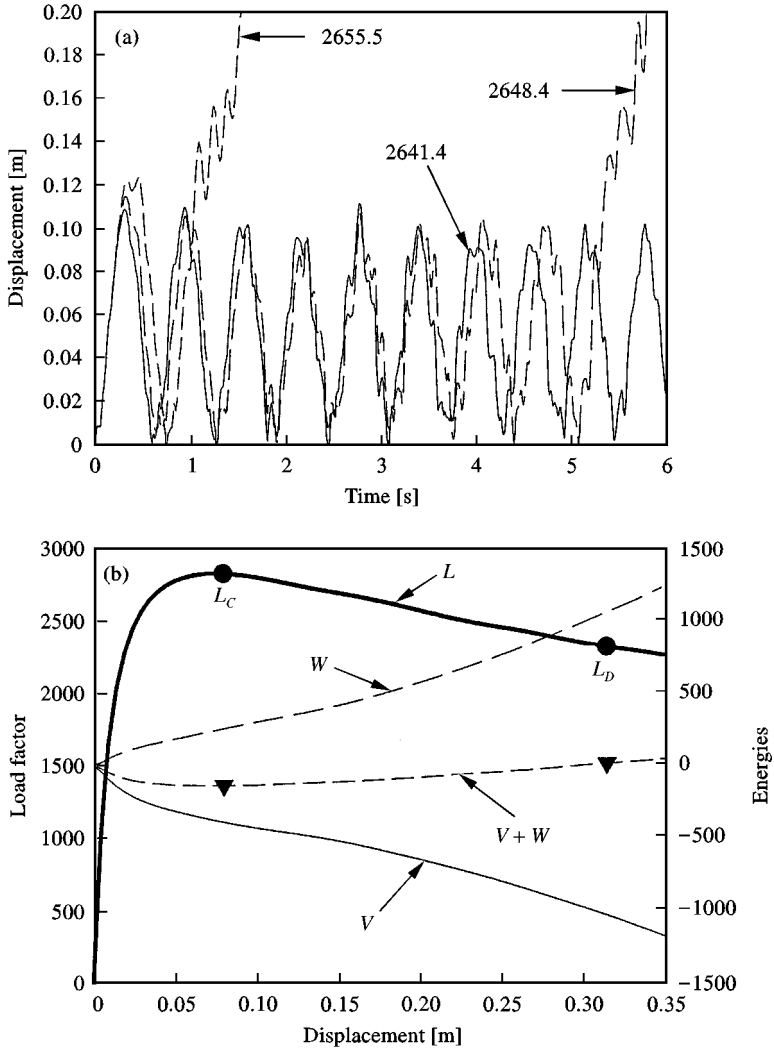

Figure 18. Imperfect short corrugated wall silo without the roof: (a) transient analysis at the leading edge for different load levels; (b) static analysis. (L) Load–displacement equilibrium path; (V) potential of the external loads; (W) internal strain energy.

The energy criterion is applicable in this problem, but leads to a low estimate ($\Lambda = 2430$).

Finally the same case has been studied with imperfections of 5 mm amplitude in the form of the static buckling mode. The dynamic response in Figure 18(a) becomes unstable at $\Lambda = 2655$ and approximately 1 s. The static response in Figure 18(b) has a maximum at $\Lambda = 2825$, while the energy estimate leads to $\Lambda = 2313$.

10. CONCLUSIONS

Under the simulation of wind pressure and step or impulsive load, the present studies show that the forced vibrations of the system lead to an unstable response.

This occurs for both complete silos and for silos without the roof, but in the latter case the load required is much less than that for the complete silo. Loss of the roof may imply a 50% reduction in the carrying capacity of the silo, so that it is crucial to maintain collaboration from the roof at all times before dynamic instability of the full silo occurs.

Identification of the onset of instability is more difficult in the phase-space diagram and has not been used as stability criterion in this work. Computation of the phase space for the case studied in this paper is done only as an illustration of the cycles that occur before instability. A more refined load step (involving many computations) is required to identify dynamic buckling from the phase-space diagram.

The non-linear static studies provide a good estimate to the instability following forced vibrations of the system. The differences obtained for typical silo geometry are less than 5%. This indicates that inertia effects are not very significant for this class of problems.

The energy criterion of step load buckling is not applicable for the case of complete silos studied. The only problem in which this simplified estimate was possible to be computed was in the silo without the roof, in which case the estimates were too conservative.

Finally, linear bifurcation buckling is a reasonable approximation to the silo of Section 3, but was overconservative for silos constructed with corrugated walls.

The results of this appear seem to reinforce the idea tht wind load buckling of silos needs to be investigated using the forced vibration response of the shell, and that acceptable estimates can be obtained by means of a static non-linear analysis under the same pressure distribution. The static analysis is also of great value in the identification of the load range for which the forced vibrations are to be studied.

ACKNOWLEDGEMENTS

The authors are members of the scientific staff of CONICET (Science Research Council of Argentina). Support for this project was provided by grants from CONICET, CONICOR (Science Research Council of Córdoba) and SECYT-UNC (National University of Córdob, Argentina).

REFERENCES

1. Y. Wang and D. P. Billington 1974 *Journal of engineering mechanics division ASCE* 1005–1023. Buckling of cylindrical shells by wind pressures.
2. B. P. Holownia 1964 *Structures and Materials Note*, 292, *Australian Department of Supply*. Buckling of cylindrical shells under wind loading.
3. H. L. Langhaar and R. E. Miller 1967, *Proceedings Symposium on the Theory of Shells, University of Houston, TX*. Buckling of an elastic isotropic cylindrical shell subjected to wind pressure.
4. T. H. G. Megson, J. Harrop and M. N. Miller 1987 *Stability of Plate and Shell Structures, Ghent University, Ghent*, 529–538. The stability of large diameter thin-walled tanks subjected to wind loading.

5. G. J. Simitses 1990 *Dynamic Buckling of Suddenly Loaded Structures*, New York: Springer-Verlag.
6. A. T. Brewer and L. A. Godoy 1996 *Nonlinear Dynamics* **9**, 249–264. Dynamic buckling of discrete structural systems under combined step and static loads.
7. B. Budiansky and R. S. Roth 1962 In *Collected Papers on Stability of Shell Structures*, NASA TN-1510. Axisymmetric dynamic buckling of clamped shallow spherical shells.
8. F. G. Flores and L. A. Godoy 1998 *Engineering Structures* **20**, 750–760. Buckling of short tanks due to hurricanes.
9. F. G. Flores and L. A. Godoy 1991 In *Buckling of Shells Structures, on Land, in the Sea and in the Air* (J. F. Jullien, editor) London, Elsevier: 213–222. Instability of shells of revolution using ALREF: studies for wind loaded shells.
10. F. G. Flores and L. A. Godoy 1992 *International Journal for Numerical Methods in Engineering*, **33**, 1775–1794. Elastic postbuckling analysis via finite elements and perturbation techniques. Part I: formulation.
11. F. G. Flores and L. A. Godoy 1993 *Internal Journal for Numerical Methods in Engineering* **36**, 331–354. Elastic postbuckling analysis via finite elements and perturbation techniques. Part II: application to shells of revolution.
12. F. G. Flores 1996 *ALPHA: A Static/Dynamic Implicit Finite Element Program, User's Manual*. Córdoba, Argentina: National University of Córdoba.
13. J. C. Simo and D. D. Fox 1989 *Computer Methods in Applied Mechanics and Engineering* **72**, 267–304. On stress resultant geometrically exact shell model. Part I: formulation and optimal parametrization.
14. J. C. Simo, D. D. Fox and M. S. Rifai 1990 *Computer Methods in Applied Mechanics and Engineering* **79,** 21–70. On stress resultant geometrically exact shell model. Part III: computational aspects of the nonlinear theory.
15. J. C. Simo and J. G. Kennedy 1992 *Computer Methods in Applied Mechanics and Engineering* **96**, 133–171. On stress resultant geometrically exact shell model. Part V, nonlinear plasticity: formulation and integration algorithms.
16. J. C. Ŝimo and N. Tarnow 1994 *International Journal of Numerical Methods in Engineering* **37**, 2527–2549. A new energy and momentum conserving algorithm for the nonlinear dynamics of shells.
17. D. Briassoulis 1988 *Computers and Structures* **23**, 129–138. Equivalent orthotropic properties of corrugated sheets.
18. P. Wriggers and J. C. Simo 1990 *International Journal of Numerical Methods in Engineering* **30**, 155–176. A general procedure for the direct computation of turning and bifurcation points.
19. F. G. Flores 1996 *DELTA*: *A Explicit Finite Element Program*, *User's Manual*, Córdoba, Argentina: National University of Córdoba.
20. N. J. Hoff and V. C. Bruce 1954 *Journal of Mathematics and Physics* **32**, 276–278. Dynamic analysis of the buckling of laterally loaded flat arches.
21. G. J. Simitses, A. N. Kounadis and J. Giri 1979 *ASCE J. Engineering Mechanics Division* 105, 896–00. Dynamic buckling of simple frames under a step load.
22. C. S. Hsu 1968 *International Journal of Engineering Science* **4**, 31–39. Stability of shallow arches against snap-though under timewise step loads.
23. A. N. Kounadis and I. Raftoyiannis 1990 *AIAA Journal* **28**(7) 1217–1223. Dynamic stability criteria of nonlinear elastic damped/undamped systems under step loading.
24. W. Ruiz, Undated, *Technical Report*, *Mayaguez* (*Puerto Rico*). Investigation into the causes and effects of structural failures at Federacion Pecuaria de Puerto Rico.
25. I. Raftoyiannis and A. N. Kounadis 1988, *Dynamic and Stability of Structures*, **3**, 219–234. Dynamic buckling of limit-point system under step loading.
26. ACI-ASCE Committee 334, 1991 *Reinforced Concrete Cooling Tower Shells–Practice and Commentary* (ACI 334,2R,91). New York: American Concrete Institute.
27. R. F. Rish 1967, *Proceedings of the Institution of Civil Engineers* **36**, 791–803. Forces in cylindrical shells due to wind.

APPENDIX A: DATA FOR COMPUTATIONS

The Fourier coefficients of the circumferential variation of wind pressure have been investigated by several authors for different shell forms and dimensions. Table 1 contains values from the joint ACI-ASCE committee on cooling towers [26], and from an earlier classical work by Rish [27]. But for silos with dimensions similar to those studied in this paper it is not easy to find experimental information on wind pressures. The two sets of coefficients in Table 1 were employed in the computations and the results showed that the small differences in pressures did not produce any significant effects on the dynamic buckling results. Different distributions in height were also employed (constant and linear variations in elevation). However, the computations indicate that the actual pressure distribution is not so critical for the thin shells considered in this paper. Similar conclusions were obtained for short tanks in reference [8]. Because of the above, the results reported in this paper have been computed using the wind distribution from reference [26] and constant pressure values in elevation.

TABLE 1
Fourier coefficients of wind pressure variation

	Ref. [26]	Ref. [27]
c_0	0·2765	0·387
c_1	− 0·3419	− 0·338
c_2	− 0·5418	− 0·533
c_3	− 0·3872	− 0·471
c_4	− 0·0525	− 0·166
c_5	0·0771	0·066
c_6	0·0039	0·055
c_7	− 0·0341	